

# Expressions for Tidal Conversion at Seafloor Topography using Physical-Space Integrals

**Norbert Schorghofer**

Institute for Astronomy, 2680 Woodlawn Drive, University of Hawaii, Honolulu, Hawaii 96822

E-mail: [norbert@hawaii.edu](mailto:norbert@hawaii.edu)

**Abstract.** The barotropic tide interacts with seafloor topography to generate internal gravity waves. Equations for the streamfunction and power conversion are derived in terms of integrals over the topography in spatial coordinates. The slope of the topography does not need to be small. Explicit equations are derived up to second order in slope for general topography, and the conversion by a bell-shaped topography is calculated analytically to this order. A concise formalism using Hilbert transforms is developed, the minimally converting topographic shape is discussed, and a numerical scheme for the evaluation of power conversion is designed that robustly deals with the singular integrand.

*Keywords:* Internal gravity waves; two-dimensional fluid flow; geophysical fluid dynamics

## 1. Preliminaries

### 1.1. Introduction

Diapycnal mixing in the deep ocean is particularly high over rough seafloor topography and a potential source of the required mechanical energy is the generation and breaking of internal gravity waves (Egbert and Ray, 2000; Ledwell et al., 2000). Tidal dissipation has long been recognized as important in the shallow coasts, but theoretical estimates of the power conversion in the abyssal ocean have turned out to be less reliable (Garrett and Kunze, 2007).

A stratified fluid sustains internal gravity waves in its interior, which can be generated by the interaction of the barotropic tide with seafloor topography. Through this process, energy of the barotropic tides is converted into internal wave energy (Wunsch, 1975; Thorpe, 1975). Figure 1 illustrates the idealized setup. For a uniform density stratification, the waves propagate at a fixed angle to the horizontal. If the topographic slope is everywhere less than the direction of internal wave propagation, it is called “subcritical”.

Bell (1975a,b) has obtained an explicit formula for the power conversion from the barotropic tide to internal waves when the slope of the bottom topography is much less than the critical slope, which is known as “weak topography approximation”. This now classical expression is written in terms of the Fourier transform of the topography. Balmforth et al. (2002) have extended this approach to all subcritical topographies, also using Fourier representation. This more general case leads to an implicit equation (re-derived in section 1.4 below). They have also derived a high-order perturbative expansion for sinusoidal topography and numerically obtained conversion rates for Gaussian topography of any subcritical slope.

The effect of wave reflection on the ocean surface was considered by Llewellyn-Smith and Young (2002) and Khatiwala (2003). Baines (1973) has calculated the conversion for certain subcritical topographies, using iterative solutions to integral equations.

Physical space representation is also commonly used. Nycander (2005) has transformed Bell’s formula for the power conversion to physical space integrals. Buhler and Muller (2007) have expressed the streamfunction in terms of the Hilbert transform of the topography. Both of these results use the weak topography approximation. Here, a formalism using physical space integrals is developed for topographic slopes not necessarily much less than the angle of wave propagation. Explicit second order formulas for general topography are also derived.

In addition to the slope correction, the physical space formulas are exploited in

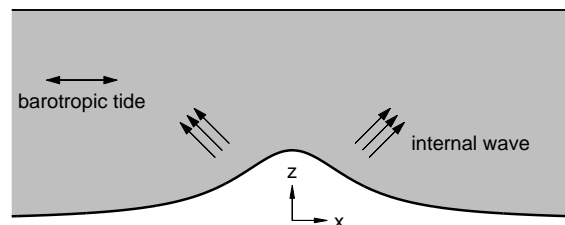


**Figure 1.** The barotropic tide generates internal waves off a seamount. The density stratification sets the angle of wave propagation.

two more lines of investigation. One is the discussion of upper and lower bounds to the power conversion in the weak topography approximation; the former leads to a simple upper bound and the latter to a surprising question about the lower bound. The last line of investigation involves discrete approximations of the physical space formulas and leads to a numerical scheme that is demonstrably robust with respect to discretization errors. With proper treatment of the singular integrand, its rate of convergence is second order in spatial resolution. This numerical scheme can be applied to the weak topography approximation, but also to second and higher order in slope.

Sections 2 and 3 cast the equations for the streamfunction and the energy conversion rate in terms of the topography in physical space  $h(x)$  instead of Fourier space  $\hat{h}(k)$ . A radiation condition is imposed in the complex plane. Upper and lower bounds for the power conversion in the weak topography approximation are also discussed. In section 4, explicit formulas up to second order in slope are derived for the conversion rate and the streamfunction. Section 5 carries through these calculations for a bell-shaped topography. Section 6 provides robust and accurate numerical schemes for the evaluation of the power conversion. The last section summarizes the results. Commonly used symbols are a hat  $\hat{\cdot}$  for the Fourier transform,  $\mathcal{H}$  for the Hilbert transform, and  $\mathcal{P}$  for the Cauchy principal value integral.

## 1.2. Model system

The starting point for the analysis are the linearized equations for an inviscid, vertically stratified and rotating fluid in the Boussinesq approximation. If there is no variation along one horizontal direction, as is approximately true along oceanic ridges, the flow can be described by a two-dimensional streamfunction  $\psi(x, z, t)$ , such that the horizontal and vertical velocities are  $u = -\psi_z$  and  $w = \psi_x$ , respectively. Subscripts indicate partial derivatives. This leads to the internal gravity wave equation (Baines, 1971; Roberts, 1975; Balmforth et al., 2002)

$$\partial_{tt}(\psi_{xx} + \psi_{zz}) + N_b^2 \psi_{xx} + f_c^2 \psi_{zz} = 0. \quad (1.1)$$

Here,  $t$  is time,  $N_b(z)$  is the buoyancy frequency, and  $f_c$  is the Coriolis parameter,  $f_c = 2\vec{\Omega} \cdot \hat{z}$ , where  $\vec{\Omega}$  is Earth's rotation vector.

Time-periodic solutions of the form  $\psi(x, z, t) = U_0 \Re(e^{-i\omega t} \varphi(x, z))$  introduce a complex function  $\varphi(x, z)$  whose phase describes the lag relative to an oscillatory motion  $\cos(\omega t)$ , where  $\omega$  is the frequency of the barotropic tide. The prefactor  $U_0$  is the velocity amplitude of the tide. With this time-dependence, equation (1.1) becomes

$$\mu^2 \varphi_{xx} = \varphi_{zz} \quad (1.2)$$

with

$$\mu^2 = \frac{N_b^2 - \omega^2}{\omega^2 - f_c^2}. \quad (1.3)$$

Equation (1.2) is hyperbolic in two spatial coordinates. Internal waves are sustained when  $\mu^2 > 0$ . The characteristics of the solution are at a slope of  $\pm 1/\mu$  relative to the horizontal, which defines a ‘‘critical’’ slope for this problem.

The barotropic tide is represented as a spatially uniform oscillatory background flow with horizontal velocity  $U_0 \cos(\omega t)$ . The role of any mean flow is ignored. Equations (1.1) and (1.2) are valid for the total streamfunction as well as the streamfunction describing the motion relative to the background tide. The total

streamfunction can be written as  $\Phi = -z + \varphi$ ;  $\Phi$  describes the motion relative to the ground, while  $\varphi$  describes the motion relative to the background tide.

At the bottom of the ocean, the velocity is tangential to the topography  $h(x)$ . This yields  $\Phi(x, h(x)) = 0$  or

$$\varphi(x, h(x)) = h(x) \quad (1.4)$$

as a lower boundary condition.

By rotation of the coordinate system, it can be shown that any solution to equation (1.2) is of the form

$$\varphi(x, z) = f(x + \mu z) + g(x - \mu z), \quad (1.5)$$

where  $f$  and  $g$  are complex-valued functions of one variable. The characteristics are at a slope of  $\pm 1/\mu$  relative to the horizontal, which defines the critical slope.

### 1.3. Energy flux and upper radiation boundary condition

Throughout, Fourier transform and inverse Fourier transform are defined with the following prefactors and signs,

$$\hat{h}(k) = \int_{-\infty}^{\infty} dx h(x) e^{-ikx} \quad \text{and} \quad h(x) = \frac{1}{2\pi} \int_{-\infty}^{\infty} dk \hat{h}(k) e^{ikx} \quad (1.6)$$

Assuming the functions  $f$  and  $g$  can be represented by their Fourier transforms  $\hat{f}$  and  $\hat{g}$ , (1.5) becomes

$$\varphi(x, z) = \frac{1}{2\pi} \int_{-\infty}^{\infty} dk \left[ \hat{f}(k) e^{ik(x+\mu z)} + \hat{g}(k) e^{ik(x-\mu z)} \right]. \quad (1.7)$$

The energy due to the velocity and buoyancy of fluid parcels leads to an expression for the energy flux. Since it is derived, for example, in Balmforth et al. (2002), we only note here the resulting expression for the time averaged vertical energy flux,

$$J(x, z) = -\frac{\rho_0 U_0^2}{2\omega} (\omega^2 - f_c^2) \Im(\varphi^* \varphi_z). \quad (1.8)$$

The asterisk (\*) indicates complex conjugation. Using Fourier representation (1.7),

$$\begin{aligned} \varphi^* \varphi_z &= \frac{1}{(2\pi)^2} \int_{-\infty}^{\infty} dk \int_{-\infty}^{\infty} dk' e^{i(k'-k)x} \\ &\quad \times \left[ \hat{f}^*(k) e^{-ik\mu z} + \hat{g}^*(k) e^{ik\mu z} \right] ik' \mu \left[ \hat{f}(k') e^{ik'\mu z} - \hat{g}(k') e^{-ik'\mu z} \right]. \end{aligned} \quad (1.9)$$

When integrated over all  $x$ , along any transect higher than the highest point of the bottom topography, only  $k' = k$  contributes to the integral over  $x$ , hence

$$\int_{-\infty}^{\infty} dx \varphi^* \varphi_z = \frac{i\mu}{2\pi} \int_{-\infty}^{\infty} dk k \left[ |\hat{f}(k)|^2 - |\hat{g}(k)|^2 + 2i \Im(\hat{f}(k) \hat{g}^*(k) e^{2ik\mu z}) \right]. \quad (1.10)$$

Only the imaginary part of this expression is needed for the energy flux, which is independent of  $z$ , and it is unnecessary to take  $z \rightarrow \infty$ . The total power conversion is the total upward energy flux

$$\begin{aligned} P &= \int_{-\infty}^{\infty} dx J(x, z) \\ &= \frac{\rho_0 U_0^2}{2\omega} \sqrt{(N_b^2 - \omega^2) (\omega^2 - f_c^2)} \int_{-\infty}^{\infty} \frac{dk}{2\pi} k \left[ |\hat{g}(k)|^2 - |\hat{f}(k)|^2 \right]. \end{aligned} \quad (1.11)$$

It is convenient to abbreviate (twice) the prefactor as

$$C \equiv \frac{\rho_0 U_0^2}{2\pi\omega} \sqrt{(N_b^2 - \omega^2)(\omega^2 - f_c^2)}. \quad (1.12)$$

According to (1.11) there are “outgoing waves” with a positive contribution to the energy flux,  $\hat{g}(k > 0)$  and  $\hat{f}(k < 0)$ , and “incoming waves” with a negative contribution to the energy flux,  $\hat{g}(k < 0)$  and  $\hat{f}(k > 0)$ . The radiation boundary condition is

$$\hat{g}(k < 0) = 0 \quad \text{and} \quad \hat{f}(k > 0) = 0, \quad (1.13)$$

which eliminates the incoming waves.

#### 1.4. Solution in Fourier representation

It is convenient to redefine the coefficients as  $\hat{b}(k) = \hat{f}(k)$  when  $k \leq 0$  and  $\hat{b}(k) = \hat{g}(k)$  when  $k \geq 0$ , and to rewrite (1.7) as

$$\varphi(x, z) = \frac{1}{2\pi} \int_{-\infty}^{\infty} dk \hat{b}(k) e^{i(kx - \mu|k|z)}. \quad (1.14)$$

At  $z = 0$  this equation reads

$$\varphi(x, 0) = \frac{1}{2\pi} \int_{-\infty}^{\infty} dk \hat{b}(k) e^{ikx} = b(x), \quad (1.15)$$

which leads to a simple interpretation of  $b(x)$  as the streamfunction at zero height; compare with (1.4). With boundary condition (1.4) one arrives at the integral equation

$$h(x) = \frac{1}{2\pi} \int_{-\infty}^{\infty} dk \hat{b}(k) e^{i(kx - \mu|k|h(x))} \quad (1.16)$$

to be solved for the unknown function  $\hat{b}(k)$ . From (1.11)

$$P = C \int_0^{\infty} dk k |\hat{b}(k)|^2. \quad (1.17)$$

This reproduces a result in Balmforth et al. (2002).

If  $\mu$  is small and  $\mu h(x)$  is neglected in the exponential of (1.16), then (1.16) reduces to an inverse Fourier transform, and the solution is simply  $\hat{b}(k) = \hat{h}(k)$ . According to (1.17), the power conversion becomes

$$P_w = C \int_0^{\infty} dk k |\hat{h}(k)|^2. \quad (1.18)$$

Since our topography is two-dimensional, the conversion rate has to be multiplied with the length of the topography (in  $y$ -direction) to obtain the total power conversion. This formula is essentially the result of Bell (1975a). The subscript  $w$  stands for “weak topography approximation”.

## 2. Physical-Space Solution for Finite Topography

### 2.1. $f(x)$ in terms of $b(x)$

The goal of the following calculation is to find expressions for  $f(\zeta)$  and  $g(\zeta)$  in terms of  $b(x)$  with all boundary conditions imposed, which then provides the streamfunction by means of (1.5).

The first step is to relate  $f(x)$  and  $g(x)$  to  $\hat{b}(k)$ . From (1.5)

$$\varphi\left(\frac{\zeta}{2}, \frac{\zeta}{2\mu}\right) = f(\zeta) + g(0) \quad \text{and} \quad \varphi\left(\frac{\zeta}{2}, -\frac{\zeta}{2\mu}\right) = f(0) + g(\zeta) \quad (2.1)$$

and using (1.14)

$$f(\zeta) = \frac{1}{2\pi} \int_{-\infty}^0 dk \hat{b}(k) e^{ik\zeta} \quad \text{and} \quad g(\zeta) = \frac{1}{2\pi} \int_0^{\infty} dk \hat{b}(k) e^{ik\zeta} \quad (2.2)$$

The inverse Fourier transform of  $\hat{b}(k)$  introduces  $b(x)$ ,

$$f(\zeta) = \frac{1}{2\pi} \int_{-\infty}^{\infty} dx b(x) \int_{-\infty}^0 dk e^{ik(\zeta-x)} = \frac{1}{2\pi} \int_{-\infty}^{\infty} dx b(x) \int_0^{\infty} dk e^{-ik(\zeta-x)} \quad (2.3)$$

$$g(\zeta) = \frac{1}{2\pi} \int_{-\infty}^{\infty} dx b(x) \int_0^{\infty} dk e^{ik(\zeta-x)} \quad (2.4)$$

It is convenient to define two kernels

$$I_f(x, \zeta) = \int_0^{\infty} dk e^{ik(-\zeta+x)} \quad \text{and} \quad I_g(x, \zeta) = \int_0^{\infty} dk e^{ik(\zeta-x)} \quad (2.5)$$

such that

$$f(\zeta) = \frac{1}{2\pi} \int_{-\infty}^{\infty} dx b(x) I_f(x, \zeta) \quad \text{and} \quad g(\zeta) = \frac{1}{2\pi} \int_{-\infty}^{\infty} dx b(x) I_g(x, \zeta) \quad (2.6)$$

Since the kernels diverge at  $\zeta = x$ , it is necessary to regularize the integral. This is done with the radiation condition (Carrier et al., 1966; Lighthill, 1978), by moving the singular points slightly away from the real axis. Physically, the shifting of the poles can be thought of as a gradual decay of the wave amplitude with distance from the internal wave beams. Either sign for the shift can be experimented with

$$I_f(x, \zeta \mp i\epsilon) = \int_0^{\infty} dk e^{ik(-\zeta \pm i\epsilon + x)} = \frac{1}{i} \left. \frac{e^{ik(x-\zeta \pm i\epsilon)}}{x - \zeta \pm i\epsilon} \right|_{k=0}^{\infty} \quad (2.7)$$

The upper integration boundary is

$$-i \lim_{A \rightarrow \infty} \frac{e^{\mp A\epsilon} e^{iA(x-\zeta)}}{x - \zeta \pm i\epsilon} \quad (2.8)$$

Only the upper sign ( $\epsilon > 0$ ) yields finite results. Therefore we define the regularized kernel as  $I_f(x, \zeta - i\epsilon)$  and take the limit  $\epsilon \rightarrow 0^+$  after the integration. From the lower integration boundary in (2.7)

$$I_f(x, \zeta - i\epsilon) = -\frac{1}{i} \frac{1}{x - \zeta + i\epsilon} \quad (2.9)$$

The result is thus

$$f(\zeta) = \frac{i}{2\pi} \lim_{\epsilon \rightarrow 0^+} \int_{-\infty}^{\infty} dx \frac{b(x)}{x - \zeta + i\epsilon} \quad (2.10)$$

The analogous calculation for  $g$  leads to a regularized kernel of the form  $I_g(x, \zeta + i\epsilon)$  and

$$g(\zeta) = \frac{i}{2\pi} \lim_{\epsilon \rightarrow 0^+} \int_{-\infty}^{\infty} dx \frac{b(x)}{-x + \zeta + i\epsilon} \quad (2.11)$$

Equation (2.10) can be recast in a more convenient form by means of a principal value integral, denoted with  $f$ . Contour integration around a counter-clockwise circle  $D$  centered at  $x = \zeta - i\epsilon$  gives

$$\int_D dx \frac{b(x)}{x - \zeta + i\epsilon} = 2\pi i b(\zeta - i\epsilon) \quad (2.12)$$

The principal value is the average of a path along the real axis and a path with a semi-circle around the pole. Thus, the principal value and the limit integral differ by half of this contribution,

$$\int_{-\infty}^{\infty} dx \frac{b(x)}{x - \zeta} = \lim_{\epsilon \rightarrow 0^+} \int_{-\infty}^{\infty} dx \frac{b(x)}{x - \zeta + i\epsilon} + i\pi b(\zeta) \quad (2.13)$$

Hence, (2.10) can be reformulated as

$$f(\zeta) = \frac{1}{2}b(\zeta) + \frac{i}{2\pi} \int_{-\infty}^{\infty} dx \frac{b(x)}{x - \zeta} \quad (2.14)$$

The analogous calculation for  $g$  leads to

$$g(\zeta) = \frac{1}{2}b(\zeta) - \frac{i}{2\pi} \int_{-\infty}^{\infty} dx \frac{b(x)}{x - \zeta} \quad (2.15)$$

In the weak topography approximation,  $b$  is real and the real and imaginary parts of (2.14) and (2.15) can be expressed separately as

$$\Re f_w(\zeta) = \Re g_w(\zeta) = \frac{1}{2}h(\zeta) \quad (2.16)$$

$$\Im f_w(\zeta) = -\Im g_w(\zeta) = \frac{1}{2\pi} \int_{-\infty}^{\infty} dx \frac{h(x)}{x - \zeta} \quad (2.17)$$

where  $f_w$  and  $g_w$  are the weak topography limits of  $f$  and  $g$ , respectively. We have  $g_w = f_w^*$ .

It is convenient to define the functional

$$\mathcal{H}[b](\zeta) \equiv \int_{-\infty}^{\infty} dx \frac{b(x)}{x - \zeta} \quad (2.18)$$

$\mathcal{H}$  is known as Hilbert transform, often also defined with a prefactor of  $-1/\pi$ . The results (2.14) and (2.15) can then be succinctly written as

$$2f(\zeta) = b(\zeta) + \frac{i}{\pi} \mathcal{H}[b](\zeta) \quad \text{and} \quad 2g(\zeta) = b(\zeta) - \frac{i}{\pi} \mathcal{H}[b](\zeta) \quad (2.19)$$

In the weak topography approximation ( $b = h$ ), this result has been derived by Buhler and Muller (2007).

## 2.2. Equation for $b(x)$

With the help of (2.19), the lower boundary condition (1.4) reads

$$h(x) = f(x + \mu h(x)) + g(x - \mu h(x)) \quad (2.20)$$

$$\begin{aligned} &= \frac{1}{2}b(x + \mu h(x)) + \frac{1}{2}b(x - \mu h(x)) \\ &\quad + \frac{i}{2\pi}\mathcal{H}[b](x + \mu h(x)) - \frac{i}{2\pi}\mathcal{H}[b](x - \mu h(x)) \end{aligned} \quad (2.21)$$

Equation (2.21) needs to be solved for the complex-valued function  $b$ . If desired, it can be rewritten as

$$h(x) = \frac{1}{2}b(x - \mu h(x)) + \frac{1}{2}b(x + \mu h(x)) + i\frac{\mu h(x)}{\pi} \int_{-\infty}^{\infty} dx' \frac{b(x')}{(x' - x)^2 - (\mu h(x))^2} \quad (2.22)$$

This integro-functional equation is the physical space representation of the integral equation (1.16).

Its validity is limited to subcritical slopes, because supercritical slopes lead to a discontinuity in the streamfunction. Below this discontinuity, the streamfunction does not need to be of the form (1.14) and thus (2.21) no longer holds for all  $x$ .

While  $b$  has a real and imaginary part, the imaginary part of  $h$  vanishes; (2.21) represents two equations, one for the real and the other for the imaginary part.

Equation (2.22) has the inversion symmetry discussed by Balmforth et al. (2002). When  $h(x) \rightarrow -h(x)$ , then  $b$  is minus the complex conjugate,

$$b[-h] = -b^*[h]. \quad (2.23)$$

It will turn out that (2.23) leaves the power conversion invariant.

Lastly, a remark about symmetric topography. It is readily shown that in (2.21) an even  $b$  will guarantee that  $h$  is even. Since all boundary conditions have been incorporated, the solution should be unique. Hence, if  $h$  is even, then  $b$  must be even. Moreover, for symmetric topography  $g(\xi) = f(-\xi)$ .

## 2.3. Some relevant properties

It is worthwhile to note some of the properties of the Hilbert transform (2.18) used in the following (King, 2009):

$$\int dx q_1(x) \mathcal{H}[q_2](x) = - \int dx \mathcal{H}[q_1](x) q_2(x) \quad (\text{anti-self-adjoint}) \quad (2.24)$$

$$\mathcal{H}'[q] = \mathcal{H}[q'] \quad (\text{differentiation}) \quad (2.25)$$

$$\mathcal{H}[\mathcal{H}[q]] = -\pi^2 q \quad (\text{inverse Hilbert transform}) \quad (2.26)$$

$$\mathcal{H}[q(ax)](\zeta) = \mathcal{H}[q(x)](a\zeta) \quad \text{for } a > 0 \quad (\text{dilation}) \quad (2.27)$$

The relation to the Fourier transform is

$$\widehat{\mathcal{H}[q]}(k) = -i\pi \text{sgn}(k) \hat{q}(k) \quad (2.28)$$

According to (2.19),  $f$  and  $g$  may be viewed as projections of  $b$ , because  $\mathcal{T}_+ \equiv \frac{1}{2}(1 + i\mathcal{H}/\pi)$  and  $\mathcal{T}_- \equiv \frac{1}{2}(1 - i\mathcal{H}/\pi)$  are projection operators. They have the properties  $\mathcal{T}_+[\mathcal{T}_+[q]] = \mathcal{T}_+[q]$  and  $\int dx q_1^*(x) \mathcal{T}_+[q_2](x) = \int dx \mathcal{T}_+^*[q_1](x) q_2(x)$ . Likewise for  $\mathcal{T}_-$ . The streamfunction can be written as

$$\varphi(x, z) = \mathcal{T}_+[b](x + \mu z) + \mathcal{T}_-[b](x - \mu z). \quad (2.29)$$

Applying the Hilbert transform again to (2.19) yields  $\mathcal{H}[f] = -i\pi f$ , meaning  $f$  is always an eigenfunction of the Hilbert transform operator. Likewise,  $\mathcal{H}[g] = +i\pi g$ .

### 3. Power Conversion in Physical-Space Representation

#### 3.1. Power conversion in terms of $f(x)$

For the vertical energy flux (1.8), the following term is needed,

$$\begin{aligned} \int_{-\infty}^{\infty} dx \varphi^*(x, z) \varphi_z(x, z) &= \int_{-\infty}^{\infty} dx [f^*(x + \mu z) + g^*(x - \mu z)] \mu [f'(x + \mu z) - g'(x - \mu z)] \\ &= \mu \int_{-\infty}^{\infty} d\xi [f^*(\xi) f'(\xi) - g^*(\xi) g'(\xi) \\ &\quad - f^*(\xi) g'(\xi - 2\mu z) + g^*(\xi - 2\mu z) f'(\xi)] \end{aligned} \quad (3.1)$$

After product integration of the last of the four terms, it is apparent that the two cross-terms are complex conjugates of each other and add up to a real function. The imaginary part is thus,

$$\Im \int_{-\infty}^{\infty} dx \varphi^*(x, z) \varphi_z(x, z) = \mu \Im \int_{-\infty}^{\infty} d\xi [f^*(\xi) f'(\xi) - g^*(\xi) g'(\xi)] \quad (3.2)$$

The total rate of energy conversion is

$$P = \int_{-\infty}^{\infty} dx J(x, z) = -\pi C \Im \int_{-\infty}^{\infty} d\xi [f^*(\xi) f'(\xi) - g^*(\xi) g'(\xi)] \quad (3.3)$$

#### 3.2. Power conversion to leading order

Here, the power conversion is expressed in terms of  $h(x)$  in the weak topography approximation, leaving the more general case to the subsequent section. According to (3.3) the term  $\Im(f^* f')$  is needed to calculate the power conversion. Using (2.14) with  $b = h$ ,

$$4f^*(\zeta) f'(\zeta) = \left[ h(\zeta) - \frac{i}{\pi} \int_{-\infty}^{\infty} dx \frac{h(x)}{x - \zeta} \right] \left[ h'(\zeta) + \frac{i}{\pi} \frac{d}{d\zeta} \int_{-\infty}^{\infty} dx \frac{h(x)}{x - \zeta} \right] \quad (3.4)$$

Upon multiplication

$$\Im(f^*(\zeta) f'(\zeta)) = \frac{1}{4\pi} \left[ -h'(\zeta) \int_{-\infty}^{\infty} dx \frac{h(x)}{x - \zeta} + h(\zeta) \frac{d}{d\zeta} \int_{-\infty}^{\infty} dx \frac{h(x)}{x - \zeta} \right] \quad (3.5)$$

Integration by parts can be applied for the integration with respect to  $\zeta$ , which undoes the  $\zeta$ -derivative in the second of the two terms. The integral of (3.5) becomes

$$\int_{-\infty}^{\infty} d\zeta \Im(f^*(\zeta) f'(\zeta)) = -\frac{1}{2\pi} \int_{-\infty}^{\infty} d\zeta h'(\zeta) \int_{-\infty}^{\infty} dx \frac{h(x)}{x - \zeta} \quad (3.6)$$

In the weak topography approximation  $g = f^*$ . Collecting the prefactor from (3.3),

$$P_w = C \int_{-\infty}^{\infty} d\zeta h'(\zeta) \int_{-\infty}^{\infty} dx \frac{h(x)}{x - \zeta} = C \int_{-\infty}^{\infty} d\zeta h'(\zeta) \mathcal{H}[h](\zeta) \quad (3.7)$$

This is the physical space representation of Bell's formula (1.18).

Comparison of (1.18) with (3.7) yields the following mathematical identity valid for the boundary conditions appropriate in our context

$$\int_0^{\infty} dk k |\hat{h}(k)|^2 = \int_{-\infty}^{\infty} d\zeta h'(\zeta) \int_{-\infty}^{\infty} dx \frac{h(x)}{x - \zeta} \quad (3.8)$$

This relation could have also been derived by deconvolution of (1.18) using (2.28).

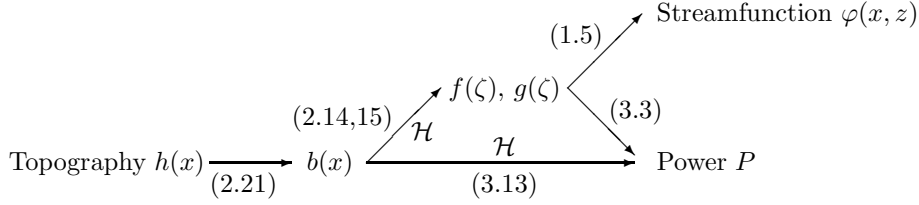


**Figure 2.** Diagrammatic summary of relations in the physical space formalism. In the weak topography approximation  $b = h$ .

### 3.3. Power conversion in terms of $b(x)$

Using the general expressions (2.19) and proceeding as in section 3.2,

$$4f^*(\zeta)f'(\zeta) = \left[ b^*(\zeta) - \frac{i}{\pi} \mathcal{H}[b^*](\zeta) \right] \left[ b'(\zeta) + \frac{i}{\pi} \frac{d}{d\zeta} \mathcal{H}[b](\zeta) \right] \quad (3.9)$$

$$4g^*(\zeta)g'(\zeta) = \left[ b^*(\zeta) + \frac{i}{\pi} \mathcal{H}[b^*](\zeta) \right] \left[ b'(\zeta) - \frac{i}{\pi} \frac{d}{d\zeta} \mathcal{H}[b](\zeta) \right] \quad (3.10)$$

Hence,

$$f^*(\zeta)f'(\zeta) - g^*(\zeta)g'(\zeta) = \frac{i}{2\pi} \left[ b^*(\zeta) \frac{d}{d\zeta} \mathcal{H}[b](\zeta) - b'(\zeta) \mathcal{H}[b^*](\zeta) \right] \quad (3.11)$$

Partial integration of the first term yields the complex conjugate of the second term,

$$\int d\zeta [f^*(\zeta)f'(\zeta) - g^*(\zeta)g'(\zeta)] = -\frac{i}{\pi} \Re \int d\zeta b'(\zeta) \mathcal{H}[b^*](\zeta) \quad (3.12)$$

Using (3.3) and (3.12), the general expression for power conversion in terms of  $b$  is thus,

$$P = C \Re \int_{-\infty}^{\infty} d\zeta b'(\zeta) \mathcal{H}[b^*](\zeta) = C \Re \int_{-\infty}^{\infty} d\zeta b'(\zeta) \int_{-\infty}^{\infty} dx \frac{b^*(x)}{x - \zeta} \quad (3.13)$$

In the weak topography approximation, this obviously reproduces (3.7). Equation (3.13) captures the power carried upward by the wave field above the highest point of the topography.

The diagram in Figure 2 illustrates relations between variables derived so far.

### 3.4. Upper and lower bounds

The following equality holds for the Hilbert transform (King, 2009),

$$\|\mathcal{H}[q]\|_2 = \pi \|q\|_2 \quad (3.14)$$

where  $\|q\|_2$  denotes the  $L^2$ -norm of a real or complex-valued function  $q$ . Combined with the Cauchy-Schwarz inequality,

$$\frac{P_w}{C} \leq \left| \int d\zeta h'(\zeta) \mathcal{H}[h](\zeta) \right| \leq \|h'\|_2 \|\mathcal{H}[h]\|_2 = \pi \|h'\|_2 \|h\|_2 \quad (3.15)$$

Thus, there is a rigorous upper bound

$$P_w \leq C\pi \sqrt{\left( \int_{-\infty}^{\infty} dx |h'(x)|^2 \right) \left( \int_{-\infty}^{\infty} dx h^2(x) \right)} \quad (3.16)$$

**Table 1.** The power conversion in the weak topography approximation  $P_w$  and the upper bound (3.16) for several topographic shapes. All topographic shapes have maximum height  $h_0$  and finite maximum slope. All results are independent of the width of the topography.

shape	$h(x)/h_0$	$P_w/(Ch_0^2)$	upper bound $/(Ch_0^2)$
–	$1/(1 +  x )$	$\left(\frac{\pi^2}{4} - 1\right) \approx 1.47$	$\frac{2\pi}{\sqrt{3}} \approx 3.63$
exponential	$e^{- x }$	2	$\pi \approx 3.14$
–	$1/\sqrt{1 + x^2}$	2	$\frac{\pi^2}{2\sqrt{2}} \approx 3.49$
bell	$1/(1 + x^2)$	$\frac{\pi^2}{4} \approx 2.47$	$\frac{\pi^2}{2\sqrt{2}} \approx 3.49$
triangular	$\max(0, 1 -  x )$	$4 \ln 2 \approx 2.77$	$\frac{2\pi}{\sqrt{3}} \approx 3.63$
Gaussian	$e^{-x^2}$	$\pi \approx 3.14$	$\sqrt{\frac{\pi^3}{2}} \approx 3.94$
–	$1/(1 + x^4)$	$\frac{3\pi^2}{8} \approx 3.70$	$\frac{\sqrt{15}}{8}\pi^2 \approx 4.78$
sinc	$\sin(x)/x$	$\frac{\pi^2}{2} \approx 4.94$	$\frac{\pi^2}{\sqrt{3}} \approx 5.70$
–	$\sqrt{2}xe^{-x^2}$	$e\pi \approx 8.54$	$\frac{e}{2}\sqrt{\frac{3\pi^3}{2}} \approx 9.27$

Table 1 shows comparisons between  $P_w$  and this upper bound for nine topographic shapes. The usefulness of this bound is promising for topographies that vary slowly. Note that except for the first example, the power conversion rates rank in the same order as the upper bounds.

More generally, an inequality can also be derived for the  $L^p$ -norm,  $\|q\|_p^p \equiv \int_{-\infty}^{\infty} dx |q(x)|^p$ . The following inequality for the Hilbert transform is due to Riesz (King, 2009),

$$\|\mathcal{H}[q]\|_p \leq B(p) \|q\|_p \quad (3.17)$$

with  $B(p) = \pi \tan(\pi/(2p))$  for  $1 < p \leq 2$  and  $B(p) = \pi / \tan(\pi/(2p))$  for  $2 \leq p < \infty$ . For  $p = 2$  equality holds (3.14). The Hölder inequality

$$\int_{-\infty}^{\infty} dx |q_1 q_2| \leq \|q_1\|_p \|q_2\|_r \quad (3.18)$$

holds for  $1/p + 1/r = 1$ ,  $1 \leq p \leq \infty$ , and  $1 \leq r \leq \infty$ . Combining the inequalities of Riesz and Hölder,

$$\frac{P_w}{C} \leq \int d\zeta |h'(\zeta) \mathcal{H}[h](\zeta)| \leq \|h'\|_p \|\mathcal{H}[h]\|_r \leq B(r) \|h'\|_p \|h\|_r \quad (3.19)$$

for  $1/p + 1/r = 1$  and  $1 < p < \infty$ . Note that  $B(r) = B(p)$ . Thus, the upper bound is

$$P_w \leq CB(r) \left( \int_{-\infty}^{\infty} dx |h'(x)|^p \right)^{\frac{1}{p}} \left( \int_{-\infty}^{\infty} dx h^r(x) \right)^{\frac{1}{r}} \quad (3.20)$$

which is a generalization of (3.16). Its usefulness does not seem to surpass that of (3.16). When applied to several of the topographies in table 1, the minimum upper bound was always achieved for  $r = p = 2$ .

For what topographic shape of maximum height  $h_0$  is the power conversion the smallest? Motivated by the results of table 1, the power conversion is calculated for a family of topographies  $h(x) = 1/(1 + |x|^\alpha)$  by means of numerical evaluation of the

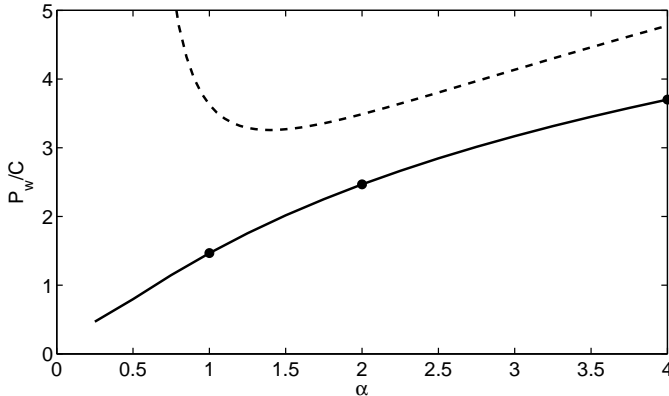


**Figure 3.** Weak power conversion for topography  $h(x) = 1/(1 + |x|^\alpha)$ . The solid line shows the numerically obtained power conversion (3.7). Solid dots are analytic results. The dashed line shows the upper bound (3.16).

Hilbert transform in (3.7). Figure 3 shows the results. With decreasing  $\alpha$  the power conversion becomes smaller and appears to approach zero. It can be hypothesized that the minimum power conversion for topographies of fixed maximum height is zero, which is physically unreasonable. However, for  $\alpha < 1$  the derivative is unbounded and thus the weak topography approximation is certain to break down. The lowest power conversion found so far among topographies with bounded derivatives is approximately  $1.47Ch_0^2$  for  $h(x) = h_0/(1 + |x|)$ ; see first entry in table 1. Overall, no better lower bound than zero can be given at this point.

The maximum possible power conversion in the weak topography approximation is infinite, because any step continuity causes it to be infinite. Combined with the hypothesis that a topography of height  $h_0 > 0$  could have zero power conversion, it can be said that the weak topography approximation has neither a physically reasonable maximum nor a physically reasonable minimum power conversion.

#### 4. Second Order Expansion

Equations (2.21) and (3.13) can be expanded in slope, or alternatively in  $\mu$ , around the weak topography result. There may be other physical corrections that may turn out to be as large or even larger than the one considered here. The following represents only one approach to increase the accuracy of tidal conversion calculations.

##### 4.1. Expansion for streamfunction

Equation (2.21) can be solved with a perturbation series

$$b(x) = b_w(x) + \mu b_1(x) + \mu^2 b_2(x) + \dots \quad (4.1)$$

As a preparatory step, it is helpful to notice that, by Taylor expansion in  $\mu$ ,

$$\frac{1}{2}b(x + \mu h(x)) + \frac{1}{2}b(x - \mu h(x)) = b(x) + \frac{1}{2}b''(x)\mu^2 h^2(x) + O(\mu^4) \quad (4.2)$$

For the Hilbert transform,

$$\mathcal{H}[b](x \pm \mu h(x)) = \mathcal{H}[b](x) \pm \mu h(x)\mathcal{H}'[b](x) + \frac{1}{2}\mu^2 h^2(x)\mathcal{H}''[b](x) + O(\mu^3) \quad (4.3)$$

Differentiation commutes with the Hilbert transform,  $\mathcal{H}'[b] = \mathcal{H}[b']$ . The expansion of (2.21) is thus

$$h(x) = b(x) + \frac{i}{\pi}\mu h(x)\mathcal{H}[b'](x) + \frac{1}{2}b''(x)\mu^2 h^2(x) + \mathcal{O}(\mu^3) \quad (4.4)$$

To zeroth order in  $\mu$ , we set  $\mu = 0$  and recover the weak topography approximation,

$$h(x) = b_w(x) \quad (4.5)$$

After substituting the expansion (4.1) into (4.4),

$$0 = \mu b_1(x) + \mu^2 b_2(x) + \frac{i}{\pi}\mu h(x)\mathcal{H}[h' + \mu b_1'](x) + \frac{1}{2}h''(x)\mu^2 h^2(x) + \mathcal{O}(\mu^3) \quad (4.6)$$

For the first order in  $\mu$ ,

$$b_1(x) = -i\frac{h(x)}{\pi}\mathcal{H}'[h](x) \quad (4.7)$$

Since  $h'$  is real,  $b_1$  is purely imaginary. It is amusing to note that

$$P_w = -i\pi C \int_{-\infty}^{\infty} dx b_1(x) \quad (4.8)$$

The second order terms are

$$b_2(x) = -\frac{1}{2}h''(x)h^2(x) - i\frac{h(x)}{\pi}\mathcal{H}'[b_1](x) \quad (4.9)$$

Since  $b_1$  is imaginary,  $b_2$  is real.

The recursion can be continued to arbitrary order, using additional terms in the expansions (4.2) and (4.3). If desired, the streamfunction (1.5) can be obtained by virtue of (2.19) as

$$2f_n = b_n + \frac{i}{\pi}\mathcal{H}[b_n] \quad \text{and} \quad 2g_n = b_n - \frac{i}{\pi}\mathcal{H}[b_n] \quad (4.10)$$

with  $n = w, 1, 2, \dots$

#### 4.2. Expansion for power conversion

Series expansion (4.1) can be also used in (3.13),

$$\begin{aligned} \Re\{b'\mathcal{H}[b^*]\} &= \Re\{[h' + \mu b_1' + \mu^2 b_2'](\mathcal{H}[h] - \mu\mathcal{H}[b_1] + \mu^2\mathcal{H}[b_2])\} + \mathcal{O}(\mu^3) \\ &= \Re\{(h' + \mu b_1' + \mu^2 b_2')\mathcal{H}[h] - (h' + \mu b_1')\mu\mathcal{H}[b_1] + h'\mu^2\mathcal{H}[b_2]\} + \mathcal{O}(\mu^3) \\ &= (h' + \mu^2 b_2')\mathcal{H}[h] - \mu^2 b_1'\mathcal{H}[b_1] + \mu^2 h'\mathcal{H}[b_2] + \mathcal{O}(\mu^4) \end{aligned}$$

The result is

$$P = C \int_{-\infty}^{\infty} d\zeta \{h'\mathcal{H}[h] + \mu^2(b_2'\mathcal{H}[h] - b_1'\mathcal{H}[b_1] + h'\mathcal{H}[b_2]) + \mathcal{O}(\mu^4)\} \quad (4.11)$$

When the power is written as an expansion

$$P = P_w + \mu^2 P_2 + \dots \quad (4.12)$$

the zeroth order reproduces (3.7), the first order vanishes, and to second order

$$P_2 = C \int_{-\infty}^{\infty} d\zeta (b_2'\mathcal{H}[h] - b_1'\mathcal{H}[b_1] + h'\mathcal{H}[b_2]) \quad (4.13)$$

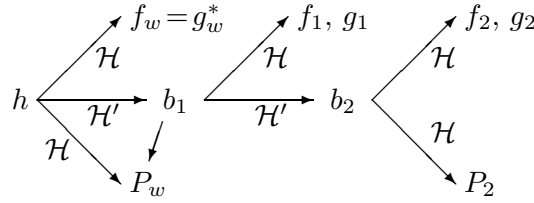


**Figure 4.** Schematic diagram showing the flow of calculation for the second order expansion based on (4.7), (4.9), (4.10), (3.7), (4.8), and (4.13). Use of the integral transforms  $\mathcal{H}$  and  $\mathcal{H}'$  is indicated.

Properties (2.24) and (2.25) and product integration can be used in (4.13) to replace  $h'\mathcal{H}[b_2]$  with  $\mathcal{H}[h]b_2'$ . Hence, the integral over the third term in (4.13) is the same as the integral over the first term. In particular, the Hilbert transform of  $b_2$  does not need to be evaluated to obtain the total power,

$$P_2 = C \int_{-\infty}^{\infty} d\zeta (2b_2' \mathcal{H}[h] - b_1' \mathcal{H}[b_1]) \quad (4.14)$$

Figure 4 illustrates relations between variables for the second order expansion.

It can be determined how the power changes as the width of the topography is stretched by a change in variable  $x \rightarrow x/\alpha$  with  $\alpha > 0$ . One quickly finds that  $\mathcal{H}[h(x/\alpha)](\zeta) = \mathcal{H}[h(x)](\zeta/\alpha)$ . The weak power conversion (3.7) is independent of slope,

$$P_w[h(x/\alpha)] = P_w[h(x)]. \quad (4.15)$$

For the second order (4.13), one arrives at

$$P_2[h(x/\alpha)] = P_2[h(x)]/\alpha^2. \quad (4.16)$$

Hence,  $P_2$  depends on the width of the topography and it does so in a simple way. When combined,

$$P_w \left[ h \left( \frac{x}{\alpha} \right) \right] + \mu^2 P_2 \left[ h \left( \frac{x}{\alpha} \right) \right] = P_w[h(x)] + \left( \frac{\mu}{\alpha} \right)^2 P_2[h(x)] \quad (4.17)$$

This result is consistent with the requirement that the power conversion be invariant under the simultaneous transformations  $x \rightarrow x/\alpha$  and  $\mu \rightarrow \mu\alpha$  to all orders.

The scaling with height can also be factored out,

$$P_w[\beta h] = \beta^2 P_w[h] \quad \text{and} \quad P_2[\beta h] = \beta^4 P_2[h] \quad (4.18)$$

If height and width change by the same factor  $\alpha = \beta$ , then  $P_w$  and  $P_2$  both change by the same factor  $\beta^2 = \beta^4/\alpha^2$ , meaning that for subcritical topography the power conversion scales with the square of the height. This scaling holds to all orders, because (2.22) is invariant under the simultaneous transformations  $x \rightarrow \alpha x$ ,  $h \rightarrow \alpha h$ , and  $b \rightarrow \alpha b$ . If the topography changes by the same factor in height and width, then  $b$  increases proportionally with  $h$ , and thus the power (3.13) is exactly proportional to the square of the height.

## 5. Example: Bell-shaped Topography

A bell shaped topography is described by

$$h(x) = \frac{s}{a^2 + x^2} \quad (5.1)$$

where  $s$  and  $a$  are parameters that determine the slope and width of the seamount. Its maximum height is  $h(0) = s/a^2$ . This topography is also known as ‘‘Witch of Agnesi’’ or Lorentzian.

### 5.1. Power conversion to zeroth order

The Hilbert transform of  $h$  is readily evaluated by contour integration in the upper-half complex plane, clockwise around pole  $x = ia$ . The principal value integral also picks up half of the contribution of the pole at  $\zeta = x$ ,

$$\begin{aligned} \int_{-\infty}^{\infty} dx \frac{s}{a^2 + x^2} \frac{1}{x - \zeta} &= 2\pi i \text{Res}(x = ia) + i\pi \text{Res}(x = \zeta) \\ &= 2\pi i \frac{1}{x - \zeta} \frac{s}{x + ia} \Big|_{x=ia} + i\pi \frac{s}{a^2 + x^2} \Big|_{x=\zeta} \\ &= 2\pi i \frac{s}{2ia} \frac{1}{ia - \zeta} + i\pi \frac{s}{a^2 + \zeta^2} \\ &= -\pi \frac{s}{a} \frac{\zeta}{\zeta^2 + a^2} \end{aligned} \quad (5.2)$$

The integration over  $\zeta$  is straightforward,

$$\int_{-\infty}^{\infty} d\zeta h'(\zeta) \int_{-\infty}^{\infty} dx \frac{h(x)}{x - \zeta} = \frac{2\pi s^2}{a} \int_{-\infty}^{\infty} d\zeta \frac{\zeta^2}{(a^2 + \zeta^2)^3} = \frac{\pi^2 s^2}{4a^4} \quad (5.3)$$

For comparison, the same result can also be obtained with the Fourier space based formalism. The Fourier transform of the topography (5.1) is  $\hat{h}(k) = \pi(s/a)e^{-a|k|}$ . Using (1.18),

$$\int_0^{\infty} dk k |\hat{h}(k)|^2 = \frac{\pi^2 s^2}{a^2} \int_0^{\infty} dk k e^{-2ak} = \frac{\pi^2 s^2}{a^2} \frac{1}{4a^2} = \frac{\pi^2 s^2}{4a^4} \quad (5.4)$$

which agrees with (5.3).

The power converted is, from (3.7) or (1.18),

$$P_w = C \frac{\pi^2 s^2}{4a^4} = C \frac{\pi^2}{4} h^2(0) \quad (5.5)$$

For comparison, the upper bound (3.16) yields

$$P_w \leq C \frac{\pi^2}{2\sqrt{2}} h^2(0) \quad (5.6)$$

This is only a factor of  $\sqrt{2}$  larger than the exact solution (5.5); see also table 1.

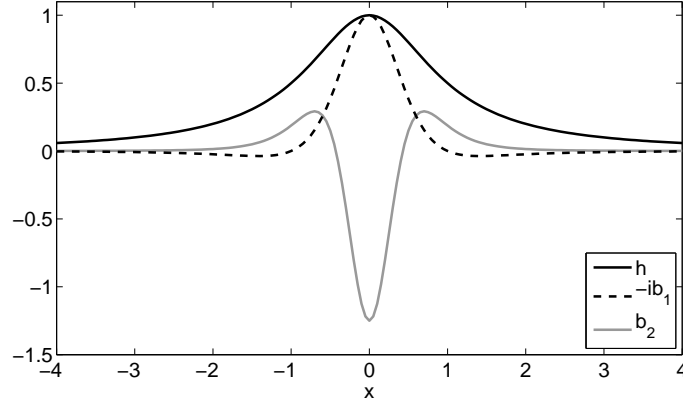


**Figure 5.** The zeroth, first, and second order result of the perturbation calculation for a bell-shaped topography with  $a = 1$  and  $h(0) = 1$ .

### 5.2. The functions $b_1$ and $b_2$

The integral in (4.7) can be evaluated by differentiation of (5.2),

$$\mathcal{H}[h'](\zeta) = \frac{\pi s}{a} \frac{\zeta^2 - a^2}{(a^2 + \zeta^2)^2} \quad (5.7)$$

The result for (4.7) is

$$b_1(x) = i \frac{s^2}{a} \frac{a^2 - x^2}{(x^2 + a^2)^3} \quad (5.8)$$

For the integral in (4.9),

$$\begin{aligned} \mathcal{H}[b'_1](x) &= \frac{d}{dx} \mathcal{H}[b_1](x) = -i\pi s^2 \frac{d}{dx} \left( x \frac{9a^4 + 2a^2x^2 + x^4}{4a^4(a^2 + x^2)^3} \right) \\ &= -i\pi s^2 \frac{9a^6 - 39a^4x^2 - a^2x^4 - x^6}{4a^4(a^2 + x^2)^4} \end{aligned} \quad (5.9)$$

The second derivative of the topography is  $h''(x) = 2s(3x^2 - a^2)/(a^2 + x^2)^3$ . According to (4.9),

$$b_2(x) = s^3 \frac{-5a^6 + 27a^4x^2 + a^2x^4 + x^6}{4a^4(a^2 + x^2)^5} \quad (5.10)$$

The graphs of  $h$ , the imaginary part of  $b_1$ , and  $b_2$  are shown in Figure 5.

### 5.3. Streamfunction up to second order

We now derive the streamfunction from  $b$  using (2.14), and verify that the lower boundary condition is satisfied. The following residuals are needed,

$$\begin{aligned} \text{Res} \left[ \frac{1}{(x^2 + a^2)(x - \zeta)} \right] (x = ia) &= \frac{1}{2ia} \frac{1}{ia - \zeta} = \frac{1}{2a} \frac{i\zeta - a}{a^2 + \zeta^2} \\ \text{Res} \left[ \frac{x^2 - a^2}{(x^2 + a^2)^3(x - \zeta)} \right] (x = ia) &= \frac{1}{2} \frac{d^2}{dx^2} \frac{x^2 - a^2}{(x + ia)^3(x - \zeta)} \Big|_{x=ia} \end{aligned} \quad (5.11)$$

$$\begin{aligned}
&= \frac{a^2 - \zeta^2}{2(a^2 + \zeta^2)^3} - i \frac{9a^4\zeta + 2a^2\zeta^3 + \zeta^5}{8a^3(a^2 + \zeta^2)^3} \quad (5.12) \\
\text{Res} \left[ \frac{-5a^6 + 27a^4x^2 + a^2x^4 + x^6}{(a^2 + x^2)^5(x - \zeta)} \right] (x = ia) &= \frac{1}{4!} \frac{d^4}{dx^4} \frac{-5a^6 + 27a^4x^2 + a^2x^4 + x^6}{(x + ia)^5(x - \zeta)} \Big|_{x=ia} \\
&= \frac{5a^6 - 27a^7\zeta^2 - a^2\zeta^4 - \zeta^6}{2(a^2 + \zeta^2)^5} \\
&\quad + i \frac{-79a^8\zeta + 50a^6\zeta^3 - 2a^2\zeta^7 - \zeta^9}{8a^3(a^2 + \zeta^2)^5}
\end{aligned}$$

$$\text{Res} \left[ \frac{1}{(x^2 + a^2)(x - \zeta)} \right] (x = \zeta) = \frac{1}{\zeta^2 + a^2} \quad (5.13)$$

$$\text{Res} \left[ \frac{x^2 - a^2}{(x^2 + a^2)^3(x - \zeta)} \right] (x = \zeta) = \frac{\zeta^2 - a^2}{(\zeta^2 + a^2)^3} \quad (5.14)$$

$$\text{Res} \left[ \frac{-5a^6 + 27a^4x^2 + a^2x^4 + x^6}{(a^2 + x^2)^5(x - \zeta)} \right] (x = \zeta) = \frac{-5a^6 + 27a^4\zeta^2 + a^2\zeta^4 + \zeta^6}{(a^2 + \zeta^2)^5} \quad (5.15)$$

The real parts of the residues all cancel when combined, leaving  $2\pi i$  times the imaginary parts,

$$\mathcal{H}[h](\zeta) = -\pi \frac{s}{a} \frac{\zeta}{a^2 + \zeta^2} \quad (5.16)$$

$$\mathcal{H}[b_1](\zeta) = -i\pi s^2 \zeta \frac{9a^4 + 2a^2\zeta^2 + \zeta^4}{4a^4(a^2 + \zeta^2)^3} \quad (5.17)$$

$$\mathcal{H}[b_2](\zeta) = \pi s^3 \zeta \frac{79a^8 - 50a^6\zeta^2 + 2a^2\zeta^6 + \zeta^8}{16a^7(a^2 + \zeta^2)^5} \quad (5.18)$$

With  $2f_n = b_n + (i/\pi)\mathcal{H}[b_n]$  and some more algebra this leads to

$$2f_w = \frac{s}{a(a + i\zeta)} \quad (5.19)$$

$$2f_1 = s^2 \frac{4ia^2 - 3a\zeta - i\zeta^2}{4a^4(a + i\zeta)^3} \quad (5.20)$$

$$2f_2 = s^3 \frac{-20a^4 - 21ia^3\zeta + 13a^2\zeta^2 + 5ia\zeta^3 - \zeta^4}{32a^7(a + i\zeta)^5} \quad (5.21)$$

or

$$\begin{aligned}
f(\zeta) &= \frac{s}{2a} \left[ \frac{1}{a + i\zeta} + s\mu \frac{4ia^2 - 3a\zeta - i\zeta^2}{4a^3(a + i\zeta)^3} \right. \\
&\quad \left. + s^2 \mu^2 \frac{-20a^4 - 21ia^3\zeta + 13a^2\zeta^2 + 5ia\zeta^3 - 3\zeta^4}{32a^7(a + i\zeta)^5} \right] + O(\mu^3) \quad (5.22)
\end{aligned}$$

Further calculation shows that

$$f(\pm x + \mu h(x)) = \frac{s}{2a} \left[ \frac{1}{a \pm ix} \pm \frac{\mu s x}{4a^3(a^2 + x^2)} \mp i \frac{\mu^2 s^2 x(x^2 - a^2)}{16a^6(a^2 + x^2)^2} \right] + O(\mu^3) \quad (5.23)$$

and thus

$$f(x + \mu h(x)) + f(-x + \mu h(x)) = \frac{s}{a^2 + x^2} + O(\mu^3) \quad (5.24)$$

or

$$\varphi(x, h(x)) = h(x) + O(\mu^3) \quad (5.25)$$

which verifies that the lower boundary condition is satisfied up to and including  $O(\mu^2)$  for the real and imaginary part.

#### 5.4. Power conversion to second order

To lowest order, the power conversion of the bell-shaped topography was obtained in (5.5). The second order can be obtained with (4.13). The Hilbert transforms are already available from (5.16), (5.17), and (5.18). After some algebra,

$$P_2 = C \frac{\pi s^4}{8a^7} \int_{-\infty}^{\infty} d\zeta \zeta^2 \frac{-148a^8 + 434a^6\zeta^2 - 2a^2\zeta^6 - \zeta^8}{(a^2 + \zeta^2)^7} = 0 \quad (5.26)$$

For this particular topography it turns out that  $P_2$  vanishes. The second order leads to spatial redistribution of the energy flux, but to no change overall.

To verify this result, it is compared with numerical solutions of the integral equation (1.16). The equation is discretized as

$$h(x_j) = \frac{1}{\pi} \sum_{\ell=0}^m \hat{b}(k_\ell) e^{-i\mu k_\ell h(x_j)} \cos(k_\ell x_j) \Delta k \quad j = 1, \dots, m \quad (5.27)$$

with  $x_j = (j - 1/2)\Delta x$ ,  $0 < x_j \leq L$ ,  $k_\ell = \ell\Delta k$ , and  $\Delta k = \pi/L$ . The number of  $k$ -modes,  $m$ , is chosen to be exactly equal the number of points along  $x$ , such that  $x_m \leq L < x_{m+1}$ . The width of the domain is  $2L$ , and the range of  $x$  chosen is only appropriate for spatially symmetric topography. This linear system turns out to be numerically well-conditioned as long as the maximum slope is subcritical and not close to critical. For consistency, the weak topography solution  $\hat{b}_w$  is obtained with the same formula, (5.27), but  $\mu = 0$ . The power is obtained with

$$P = C \sum_{\ell=1}^n k_\ell |b(k_\ell)|^2 \Delta k \quad (5.28)$$

Figure 6a demonstrates that the numerically calculated  $P_w$  agrees with the analytical solution (5.5). Even for significant slopes, the power conversion is indistinguishable from the weak topography result, verifying that  $P_2 = 0$  for the bell-shaped topography. Figure 6b demonstrates that for a Gaussian-shaped topography,  $P_2$  is no longer zero. The dashed line in figure 6b will be discussed below.

## 6. Numerical Scheme

### 6.1. Robust numerical evaluation of the weak power conversion

The goal here is to robustly and accurately evaluate equation (3.7), and especially the singular integrand in the Hilbert transform (2.18). A necessary property is reliability in the evaluation of the improper integral. Desirable properties are use of the topographic height only at measured grid points, such that interpolation is conveniently avoided, and quick evaluation computationally. All three of these properties are achieved with the following simple scheme.

Particularly useful is the concise note of Sloan (1968) that describes how the principal value integral of a function with a first order pole can be evaluated as an ordinary integral. Since

$$\oint_{-1}^1 dx \frac{1}{x - \zeta} = 0 \quad (6.1)$$

it follows that

$$\oint_{-1}^1 dx \frac{h(x)}{x - \zeta} = \int_{-1}^1 dx \frac{h(x) - h(\zeta)}{x - \zeta} \quad (6.2)$$

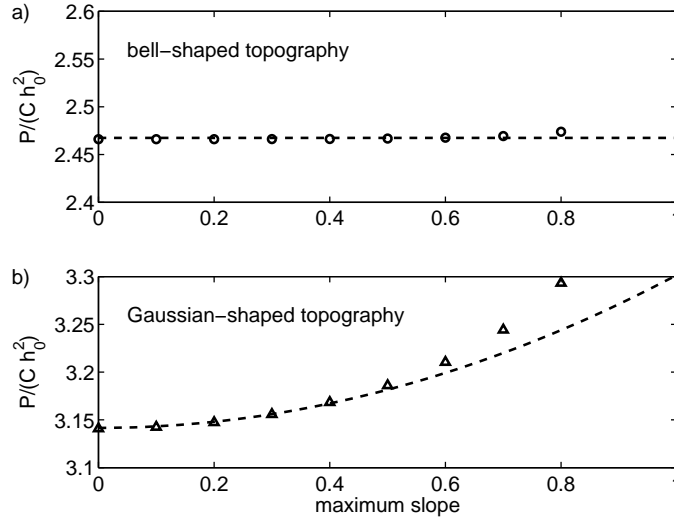


**Figure 6.** Numerically computed power conversion compared to analytical results. The horizontal axis is the maximum topographic slope relative to the critical slope. Dots show the numerically computed power conversion; dashed lines are the zeroth plus second order results. a) The higher order corrections for a bell-shaped topography are extremely small. b) The higher order corrections for a Gaussian-shaped topography do not vanish.

The right hand side is an ordinary integral, because the integrand at  $x = \zeta$  has the finite value  $h'(\zeta)$ . Hence, the transform can be evaluated numerically as an ordinary integral, with a substitution for  $x = \zeta$ . For a regularly spaced grid with separation  $\Delta x$ ,

$$\mathcal{H}[h](\zeta_\ell) = \sum_{j \neq \ell} \frac{h_j - h_\ell}{j - \ell} + h'_\ell \Delta x \quad (6.3)$$

where  $j$  and  $\ell$  are integers that enumerate the grid points up to the domain boundaries,  $\zeta_\ell = \ell \Delta x$ , and  $h_j = h(j \Delta x)$ .

The same integrand has bad convergence properties for large  $x$ , because  $\int_1^\infty dx(1/x)$  diverges. For large  $x$ , we can simply resort to the original integrand. Issues of overflow and roundoff practically disappear already one grid point away from the singularity and (6.2) only needs to be applied at the divergence itself. This leads to a concise discrete approximation for the Hilbert transform,

$$\mathcal{H}[h](\zeta_\ell) = \sum_{j \neq \ell} \frac{h_j}{j - \ell} + h'_\ell \Delta x \quad (6.4)$$

The power conversion is thus

$$P_w = C \sum_{\ell} h'_\ell \left( \sum_{j \neq \ell} \frac{h_j}{j - \ell} + h'_\ell \Delta x \right) \Delta x \quad (6.5)$$

where the prefactor was defined in (1.12). The derivative can be evaluated with a centered finite difference,

$$h'_\ell = \frac{h_{\ell+1} - h_{\ell-1}}{2\Delta x} + O(\Delta x)^2 \quad (6.6)$$

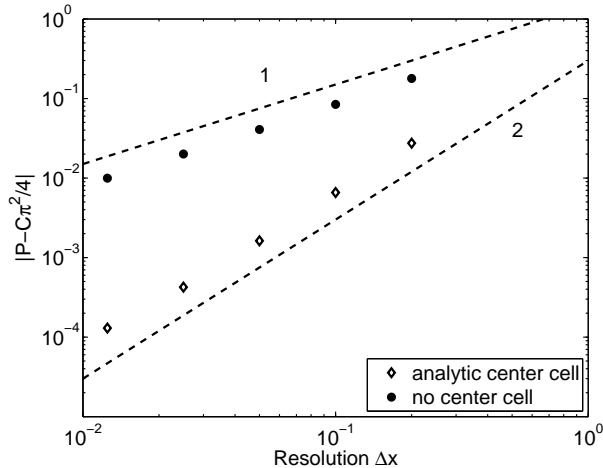


**Figure 7.** Convergence test for a bell-shaped topography with spatial resolution. The dashed lines represent linear and quadratic convergence, respectively. The numerical scheme for the evaluation of power conversion (6.5) converges with second order (diamonds). If the contribution from the singular cell is omitted (circular filled dots), the scheme still converges but only with first order. The domain width is  $L = 40a$ .

A short C program was written to evaluate the power conversion numerically with (6.5). With  $L = 40a$  and  $\Delta x = 0.02a$  it reproduces the power conversion for a bell-shaped topography to a relative accuracy of  $10^{-5}$  with respect to the analytic solution (5.5). The accuracy of the numerical evaluation depends on domain size. A relative accuracy of 1% can be achieved at  $L \sim 5a$ . For  $10^{-5}$ ,  $L \sim 40a$  is required.

This numerical scheme is also used for the calculations leading to figure 3.

### 6.2. Rate of convergence and discretization error

Figure 7 shows a convergence test for (6.5). The numerical scheme approaches the analytically known solution and converges quadratically with resolution. Without the contribution from the divergence, that is without the derivative term in (6.4), the scheme also converges, but only to first order.

The discretization error can also be discussed formally. Trapezoidal quadrature (simple summation) is extremely accurate in the interior of the domain and the dominant errors usually arise from the two boundaries. The classical Euler-Maclaurin summation formula for a smooth function  $q$  provides

$$\int dx q(x) = \sum_j q_j \Delta x + (\text{error from boundaries}) + O(\Delta x)^p \quad (6.7)$$

where  $p$  can be chosen to be two or larger. If  $q$  is analytic, then the order of the error term can be chosen arbitrarily high, meaning the discretization error from the interior of the domain is exponentially small. This is a well-known result on numerical quadrature. An extension of the Euler-Maclaurin formula to integrands with a first

order singularity is given by Lyness (1985),

$$\int dx \frac{q(x)}{x-\zeta} = \sum_j \frac{q_j}{j-\ell} + q'_\ell \Delta x + (\text{error from boundaries}) + O(\Delta x)^p \quad (6.8)$$

where again  $p$  can be at least two,  $x = j\Delta x$ , and  $\zeta = \ell\Delta x$ . In our case  $q = h$  and this formula by Lyness (1985) includes the term  $h'\Delta x$  derived above, which serves as independent verification. Once the  $q'$ -term is taken into account, discrete evaluation of the Hilbert transform enjoys about the same accuracy as discrete evaluation of an ordinary integral.

For our model, it is not rewarding to study the contribution to the integration error from the boundary points. The boundary contributions can be made arbitrarily small with sufficient domain width, but the seafloor needs to level off at exactly the same depth on both sides of the seamount, otherwise the integral does not converge at all. This problematic is already present in the governing equations and is unrelated to the discretization. Nycander (2005) has shown that corrections for an ocean of finite depth will lead to a faster decaying integrand, which alleviates this problem.

The error for a center-difference derivative is second order; see (6.6). Based on (6.8) and (6.6), the power conversion (6.5) thus converges also to second order, unless the boundary terms dominate the error. This reasoning explains the second order convergence seen in Figure 7. If in the example above, the derivative is evaluated analytically, the errors turn out to be even smaller than in figure 7. Thus, the numerical error arises in this example indeed predominantly from the numerical differentiation of  $h$ .

### 6.3. Second order numerical results

The power conversion can be obtained to second order with one more Hilbert transform (4.7) and a few numerical differentiations and integrations in (4.9) and (4.14).

Table 2 shows the numerical results for  $P_w$  and  $P_2$  obtained in this way. The values for  $P_w$  agree with those obtained analytically in Table 1. The fifth and sixth column show  $P_2$  for two different slopes related by (4.16). For example, for the Gaussian-shaped topography,

$$P \approx Ch_0^2 \left( 3.14 + 0.12\mu^2 \frac{h_0^2}{a^2} + O(\mu^4) \right) \quad (6.9)$$

$$\approx Ch_0^2 (3.14 + 0.16\mu^2 s_{\max}^2 + O(\mu^4)) \quad (6.10)$$

$$\approx P_w (1 + 0.051\mu^2 s_{\max}^2 + O(\mu^4)) \quad (6.11)$$

This result is plotted in Figure 6b in comparison to numerical solutions of the integral equation (1.16), which captures all orders. Equation (6.11) agrees with the second order correction given in Balmforth et al. (2002).

The weak power conversion diverges when either the topography has a step discontinuity or when it does not level off at equal heights on both sides of the seamount. The second order expressions lead to analogous problems when the derivative of the topography is discontinuous or when the topography decays asymptotically no faster than  $1/x$ . The topographic shapes of Table 1 that are not included in Table 2 are of this kind.

**Table 2.** Numerically obtained power conversion to zeroth and second order for several topographic shapes;  $h_0$  is the maximum height and  $s_{\max} = \max_x |h'(x)|$  is the maximum slope of the topography.

shape	$h(x)/h_0$	$s_{\max}/h_0$	$P_w/(Ch_0^2)$	$P_2/(Ch_0^2)$ $a = 1$	$P_2/(Ch_0^2)$ $s_{\max}\mu = 1$	$P_2/P_w$ $s_{\max}\mu = 1$
bell	$a^2/(a^2 + x^2)$	$3\sqrt{3}/(8a)$	2.47	0.00	0.00	0.000
Gaussian	$e^{-ax^2}$	$\sqrt{2a}/e$	3.14	0.12	0.16	0.051
–	$a^4/(a^4 + x^4)$	$3^{3/4}5^{5/4}/(16a)$	3.70	0.23	0.20	0.055
–	$\sqrt{2eaxe^{-ax^2}}$	$\sqrt{2ae}$	8.54	3.9	0.72	0.085

## 7. Summary and Discussion

Conversion from a sinusoidally varying barotropic tide into internal waves is studied in an infinitely deep ocean with uniform stratification.

Formulas for the power conversion and the streamfunction in terms of the physical space topography are derived and given by (2.21), (2.19), and (3.13). This parallels and extends previous work by Bell (1975a) and Balmforth et al. (2002) in the Fourier representation. Instead of Fourier transforms, Hilbert transforms appear in the equations. In the weak topography approximation, the power conversion in terms of physical space topography is given by (3.7).

The diagram in Figure 2 summarizes relations between important variables. Equation (2.21) relates  $h(x)$  with  $b(x)$  implicitly. It is the equivalent of integral equation (1.16) for the Fourier representation of  $b$ . In the weak topography approximation  $b = h$ . Derived from the function  $b$  can be the streamfunction with (2.19) and (1.5) or the power conversion directly with (3.13). Equation (3.13) is the physical-space version of (1.17). The Hilbert transform  $\mathcal{H}$  leads from  $b$  to  $\varphi$  and from  $b$  to  $P$ .

Explicit formulas to second order in slope are given by (4.7), (4.9), and (4.11); see Figure 4 for an overview. The derivative of the Hilbert transform, which is equivalent to the Hilbert transform of the derivative, leads to successively higher perturbative orders of the function  $b_n$ . Hence, the Hilbert transform also provides the means to perturbatively solve (2.21).

Streamfunction (5.22) and power conversion (5.26) are obtained analytically for a bell-shaped topography (5.1) up to second order in slope. The lower boundary condition for the streamfunction is verified and the second order correction to the power conversion vanishes.

Within the weak topography approximation, an upper bound to the power is given by (3.16). It is also hypothesized, on the basis of numerical calculations, that the minimum conversion rate among all topographic shapes of fixed maximum height is zero, although this should not hold beyond the weak topography approximation. Among topographies self-consistent with this approximation, the first entry in table 1 is the lowest found so far. The weak topography approximation has no physically reasonable maximum or minimum power conversion.

Numerical schemes for the robust and accurate evaluation of the power conversion to zeroth and second order are given. The scheme (6.5) for the power conversion in the weak topography approximation is a simple sum where the cell with the singular

contribution is replaced by a derivative term. Simply omitting the singular cell still leads to a formula that converges, albeit only to first order. The full formula improves the accuracy, turning the rate of convergence from first to second order. It can be readily applied to realistic, but only one-dimensional, topographies. Table 2 shows the semi-numerical results for the second order slope corrections of four topographic shapes.

What are the relative advantages of the physical-space versus the Fourier representation? Admittedly, the Hilbert transform is singular and can be cumbersome to evaluate analytically. Some of the new results derived here only parallel those obtained with Fourier methods, such as (2.21) and (3.13). The results that previously had not been derived in any representation, such as (3.16), (4.7), (4.9), and (4.13), could have been derived with Fourier methods with about the same amount of effort. Nevertheless, seafloor topography is not periodic and the alternate formalism has the potential to be useful for modifications and generalization that are more intuitive in physical space than in Fourier space.

### Acknowledgments

I am indebted to Matthew Chasse, Samar Khatiwala, and Norman Lebovitz for discussions.

### References

- P. G. Baines. Reflexion of internal/inertial waves from bumpy surfaces. *J. Fluid Mech.*, 46:273, 1971.
- P. G. Baines. Generation of internal tides by flat-bump topography. *Deep Sea Res.*, 20:179, 1973.
- N. J. Balmforth, G. R. Ierley, and W. R. Young. Tidal conversion by subcritical topography. *J. Phys. Ocean.*, 32:2900, 2002.
- T. H. Bell. Lee waves in stratified fluid with simple harmonic time dependence. *J. Fluid Mech.*, 67:705, 1975a.
- T. H. Bell. Topographically generated internal waves in the open ocean. *J. Geophys. Res.*, 80:320, 1975b.
- O. Buhler and C. J. Muller. Instability and focusing of internal tides in the deep ocean. *J. Fluid Mech.*, 588:1–28, 2007.
- G. F. Carrier, M. Krook, and C. E. Pearson. *Functions of a Complex Variable*. McGraw Hill, New York, 1966.
- G. D. Egbert and R. D. Ray. Significant dissipation of tidal energy in the deep ocean inferred from satellite altimeter data. *Nature*, 405(6788):775–778, 2000.
- C. Garrett and E. Kunze. Internal tide generation in the deep ocean. *Annu. Rev. Fluid Mech.*, 39:57–87, 2007.
- S. Khatiwala. Generation of internal tides in an ocean of finite depth: analytical and numerical calculations. *Deep Sea Res. I*, 50:3–21, 2003.
- F. W. King. *Hilbert Transforms: Volume 1*. Cambridge University Press, 2009.
- J. R. Ledwell, E. T. Montgomery, K. L. Polzin, L. C. St Laurent, R. W. Schmitt, and J. M. Toole. Evidence for enhanced mixing over rough topography in the abyssal ocean. *Nature*, 403(6766):179–182, 2000.

- J. Lighthill. *Waves in Fluids*. Cambridge University Press, first edition, 1978.
- S. G. Llewellyn-Smith and W. R. Young. Conversion of the barotropic tide. *J. Phys. Ocean.*, 32:1554, 2002.
- J. N. Lyness. The Euler Maclaurin expansion for the Cauchy Principal Value integral. *Numer. Math.*, 46:611–622, 1985.
- J. Nycander. Generation of internal waves in the deep ocean by tides. *J. Geophys. Res.*, 110(C9):C10028, Oct. 2005. doi: 10.1029/2004JC002487.
- J. Roberts. *Internal Gravity Waves in the Ocean*. Marcel Dekker, New York, 1975.
- I. H. Sloan. The numerical evaluation of principal-value integrals. *J. Comput. Phys.*, 3:332–333, Oct. 1968.
- S. A. Thorpe. The excitation, dissipation, and interaction of internal waves in the deep ocean. *J. Geophys. Res.*, 80:328–338, 1975.
- C. Wunsch. Internal tides in the ocean. *Rev. Geophys.*, 13:167–182, 1975.